JGR Oceans

RESEARCH ARTICLE
10.1029/2019JC015834

A Satellite Era Warming Hole in the Equatorial Atlantic Ocean

Hyacinth C. Nnamchi[1,2], Mojib Latif[1], Noel S. Keenlyside[3,4], and Wonsun Park[1]

[1]GEOMAR Helmholtz Centre for Ocean Research Kiel, Kiel, Germany, [2]Department of Geography, University of Nigeria, Nsukka, Nigeria, [3]Geophysical Institute, University of Bergen and Bjerknes Centre for Climate Research, Bergen, Norway, [4]Nansen Environmental and Remote Sensing Center, Bergen, Norway

Key Points:
- Observations show small warming trends over the equatorial Atlantic in boreal summer during the satellite era
- The small trends are driven by intensified shoaling of the thermocline and damped by the surface turbulent heat fluxes
- The warming deficit reflects the interactions of intrinsic variability with external forcing

Correspondence to:
H. C. Nnamchi,
hnnamchi@geomar.de;
hyacinth.nnamchi@unn.edu.ng

Citation:
Nnamchi, H. C., Latif, M., Keenlyside, N. S., & Park, W. (2020). A satellite era warming hole in the equatorial Atlantic Ocean. *Journal of Geophysical Research: Oceans*, *125*, e2019JC015834. https://doi.org/10.1029/2019JC015834

Received 30 OCT 2019
Accepted 17 MAR 2020
Accepted article online 20 MAR 2020

The copyright line for this article was changed on 3 JUN 2020 after original online publication.

Abstract Observations during the satellite era 1979–2018 only depict small sea surface temperature (SST) trends over the Equatorial Atlantic cold tongue region in boreal summer. This lack of surface warming of the cold tongue, termed warming hole here, denotes an 11% amplification of the mean SST annual cycle. The warming hole is driven by a shoaling of the equatorial thermocline, linked to increased wind stress forcing, and damped by the surface turbulent heat fluxes. The satellite era warming deficit is not unusual during the twentieth century—similar weak trends were also observed during the 1890s–1910s and 1940s–1960s. The tendency for surface cooling appears to reflect an interaction of external forcing, which controls the timing and magnitude of the cooling, with the intrinsic variability of the climate system. The hypothesis for externally forced modulation of internal variability is supported by climate model simulations forced by the observed time-varying concentrations of atmospheric greenhouse gases and natural aerosols. These show that increased greenhouse forcing warmed the cold tongue and aerosols cooled it during the satellite era. However, internal variability, as derived from control integrations with fixed, preindustrial values of greenhouse gases and aerosols, can potentially cause larger cooling than observed during the satellite era. Large uncertainties remain on the relative roles of external forcing and intrinsic variability in both observations and coupled climate models.

Plain Language Summary The Atlantic cold tongue is a region of locally cooler ocean surface waters that develops just south of the equator in boreal summer, partly reflecting the upwelling of deep cold waters by the action of the southeasterly trade winds. Although there has been considerable global warming since the beginning of global satellite measurements in 1979, there is hardly any surface warming in the Atlantic cold tongue region during 1979–2018. This warming hole is most pronounced in boreal summer. Observations suggest that despite strong heat transfer from the atmosphere to the ocean, the upper ocean may have cooled. Climate model simulations show that variations in external forcing associated with greenhouse gases can cause warming of the cold tongue and aerosols cooling of it. However, model simulations that exclude variations in these external forcing show that the mechanisms internal to the climate system can potentially cause larger cooling than observed during the satellite era. Thus, we attribute the warming hole to a combination of internal variability and external forcing. It must be stressed, however, that understanding the relative roles of internal variability versus external forcing is greatly hampered by large errors in both the observational data sets and climate models.

1. Introduction

The tropical Atlantic has experienced substantial warming of the sea surfaces temperature (SST) since the beginning of the twentieth century (Deser et al., 2010; Li et al., 2015; Servain et al., 2014; Tokinaga & Xie, 2011). The profound warming trends, which dominate global-scale tropical atmosphere-ocean teleconnections during the satellite era since 1979 (Li et al., 2015), are attributed to rising levels of anthropogenic greenhouse gases (Bindoff et al., 2013). The stronger warming over the equatorial Atlantic and weakening of the southeasterly trade winds during the 1950–2009 period may additionally be related to anthropogenic aerosols loading over the Northern Hemisphere (Tokinaga & Xie, 2011). However, the southeasterly trade winds strengthened during more recent periods 1964–2012 and 1976–2012 (Servain et al., 2014).

Apart from atmospheric greenhouse and aerosol forcing effects, the long-term trends in the SST over equatorial Atlantic may also be modulated by internal variability of the climate system. Specifically, the roles of the meridional overturning ocean circulation and the related Atlantic Multidecadal Variability have

previously been highlighted in this context (Haarsma et al., 2008; Li et al., 2015; Martín-Rey et al., 2018; Polo et al., 2013; Svendsen et al., 2014; Yan et al., 2018).

Here we show that in contrast to the basin-scale SST warming over the tropical Atlantic described in some previous studies, there is hardly any SST warming over the central equatorial Atlantic in boreal summer during the satellite era 1979–2018. The present study, using observations, reanalysis data sets, and climate models, describes this lack of warming trends as a "warming hole"—an analogy to the warming deficit in the subtropical gyre region of the North Atlantic Ocean (Caesar et al., 2018; Drijfhout et al., 2012; Gervais et al., 2018; Rahmstorf et al., 2015)—and investigates the possible causes, internal and external. The data and statistical methods used are described in section 2; the warming hole is discussed in section 3 and the associated surface heat flux and ocean circulation changes in section 4. The relative roles of internal variability and external forcing are investigated in section 5, and the paper ends with concluding remarks in section 6.

2. Data, CMIP5 Ensembles, and Statistical Methods

This study focuses on the satellite era since 1979 with generally improved climate observations including the integration of in situ and satellite-derived measurements (Reynolds et al., 2002). Nonetheless, there are some remaining uncertainties that we characterize by using multiple observational and reanalysis data sets. We analyzed the trends of the SST, surface wind stress, and net heat flux (Q_{net}) as well as the vertical ocean temperature profiles in the equatorial Atlantic Ocean. Information on the data sets used including the spatial resolution, key references, variables, and period analyzed is listed in Table 1.

We investigate the possible roles of external forcing (greenhouse gas and aerosols) and of intrinsic variability of the climate system for the trends using an ensemble of 15 models from the Coupled Model Intercomparison Project phase 5 (CMIP5; Taylor et al., 2012). Outputs from four different experiments are used that are of interest here (Table 2), where the first realization was chosen when multiple realizations were available. The analyzed simulations are forced by (1) observed historical greenhouse gases and aerosols ("all forcing"), (2) observed historical greenhouse gases only ("GHGs"), (3) observed historical aerosols only ("aerosols"), and (4) fixed preindustrial values of GHGs and aerosols ("piControl"). The satellite era period available for the historical forcing simulations 1979–2005 was used to construct multimodel ensembles; for the piControl the ensemble was based on 300 years of integration.

For the observations and the CMIP5 ensembles, we estimated monotonic trends as the nonparametric Theil-Sen median slope (Sen, 1968; Theil, 1950) and tested for statistical significance using the Mann-Kendall rank statistic (Kendall, 1975; Mann, 1945). These nonparametric methods are less affected by outliers. The application of parametric methods (not shown) does not change our conclusions. The observational and model uncertainties are estimated using two-tailed Student t test. All statistical significance tests are marked at the 95% confidence level, except where it is stated otherwise. For consistency, all trend estimates have been scaled to 40 years irrespective of actual number of years analyzed.

3. The Warming Hole

The most striking feature of the SST trends over the tropical Atlantic during 1979–2018 is the occurrence of very weak trends, which are characterized by statistically nonsignificant trends, in the cold tongue region during boreal summer (July–September, JAS; Figures 1a and 1c). The weakest trends, termed "warming hole," appear in an extended area of the equatorial Atlantic in different data sets (Figures 2a–2f). Despite some sensitivity in the location of the warming hole to the choice of data set (Figure 2), all analyzed observational data sets show statistically nonsignificant trends in the Atlantic Niño region (Atl3; 3°S–3°N, 0°–20°W, shown by box in Figures 1a and 2a–2n) where the ensemble mean trend is 0.21 °C per 40 years (marked by dashed horizontal line in Figure 1c).

Consistent with the entire satellite era, the warming hole is also present during the 1984–2009 period (Figures 2g–2n) for which observations of the Q_{net} discussed in subsequent sections are available. By plotting the multi-data sets 95% confidence limits of the SST trends over the region 3°N to 3°S on the same axes, similar structure of warming hole is seen for the 1979–2018 and 1984–2009 periods (Figure 2o). While the two periods show cross-equatorial SST gradient and warming hole along the equator, there are large

Table 1
Information on the Data Sets Analyzed and Their Sources

	Data set	Resolution (Lat × Lon × Lev)	Reference	Variable(s)	Type	Period(s)
	Surface data sets					
1.	ERSST v5	2° × 2°	Huang et al. (2017)	SST	In situ	1979–2018
2.	COBE v2	1° × 1°	Hirahara et al. (2014)	SST	In situ	1979–2018
3.	HadISST	1° × 1°	Rayner et al. (2003)	SST	In situ	1979–2018
4.	KAPLAN	5° × 5°	Kaplan et al. (1998)	SST	In situ	1979–2018
5.	OAFLUX	1° × 1°	Yu and Weller (2007)	SST, Q_{net}	In situ/Satellite	1979–2018/1984–2009
6.	OISST v2	1° × 1°/ ¼° × ¼°	Reynolds et al. (2002)	SST	Satellite	1982–2018/1984–2009
7.	NCEP	1.9° × 1.9°	Kalnay et al. (1996)	Wind stress, Q_{net}	Reanalysis	1979–2018/1984–2009
8.	ERAI	0.75° × 0.75°	Dee et al. (2011)	Wind stress, Q_{net}	Reanalysis	1979–2018/1984–2009
9.	ERA5	0.25° × 0.25°	Hersbach et al. (2018)	Wind stress, Q_{net}	Reanalysis	1979–2018/1984–2009
10.	PATHFINDER	4 km	Kilpatrick et al. (2001)	SST	Satellite	1984–2009
11.	TROPLUX	1° × 1°	Kumar et al. (2012)	Wind stress, Q_{net}	Reanalysis, bias-corrected	1979–2018/1984–2009
	Ocean profile data sets					
12.	EN4	1° × 1° × 42	Good et al. (2013)	Temperature	In situ	1979–2018
13.	GECCO2	1° × 1° × 50	Köhl (2015)	Temperature	Reanalysis	1979–2016
14.	GODAS	0.4° × 1° × 42	Behringer et al. (1998)	Temperature	Reanalysis	1980–2018
15.	ORAS4	1° × 1° × 42	Balmaseda et al. (2013)	Temperature	Reanalysis	1979–2017
16.	ORAS5	1° × 1° × 75	Zuo et al. (2019)	Temperature	Reanalysis	1979–2017
17.	SODA331	0.5° × 0.5° × 42	Carton et al. (2018)	Temperature	Reanalysis	1980–2015

uncertainties, with some data sets (notably KAPLAN and HadISST) exhibiting smallest trends to the south of the equator, and this is more pronounced during the 1984–2009 (Figures 2i and 2j). We further analyzed the higher-resolution version of the OISST at ¼° horizontal grids and the Pathfinder SST at a horizontal grid spacing of 4 km (Figures 2m and 2n). The OISST ¼ and Pathfinder 4 km are derived from satellites that imply a good and consistent temporal observational coverage, and they both show warming deficit in the warming hole region. Compared to the OISST 1° × 1°, the warming hole is more clearly defined along the equator in OISST ¼°, suggesting that increasing the resolution enhances representation of the SST trends. Although the high 4 km resolution of the Pathfinder data set reveals quite noisy pattern, there is an overall good spatial agreement between the two satellite data sets.

We now focus on the Atl3 region, as it is a key index of the equatorial Atlantic interannual climate variability (Foltz et al., 2019; Keenlyside & Latif, 2007; Lübbecke et al., 2018; Zebiak, 1993). Following the mean annual cycle (Figure 1b), the Atl3 SST trends decline systematically from January–March (JFM) to April–June (AMJ) and JAS and then increase in October–December (OND) in observations (Figure 1d). The largest seasonal decline occurs between boreal spring and summer (from 0.5 ± 0.12 °C per 40 years in AMJ to

Table 2
List of the Models Used to Construct the CMIP5 Ensembles Analyzed

	CMIP5 model	Ocean grids (Lat × Lon × Lev)	Reference
1.	BCC-CSM1	232 × 360 × 40	Xin et al. (2013)
2.	CanESM2	192 × 256 × 40	Arora et al. (2011)
3.	CCSM4	320 × 384 × 60	Gent et al. (2011)
4.	CNRM-CM5	362 × 292 × 42	Voldoire et al. (2013)
5.	CSIRO-Mk3-6-0	189 × 192 × 31	Rotstayn et al. (2012)
6.	GFDL-CM3	200 × 360 × 50	Delworth et al. (2006)
7.	GFDL-ESM 2 M	200 × 360 × 50	Dunne et al. (2012)
8.	GISS-E2-H	90 × 144 × 26	Schmidt et al. (2006)
9.	GISS-E2-R	90 × 144 × 32	Schmidt et al. (2006)
10.	HadGEM2-ES	216 × 360 × 40	Collins et al. (2011)
11.	IPSL-CM5A-LR	149 × 182 × 31	Dufresne et al. (2013)
12.	MIROC-ESM	196 × 256 × 44	Watanabe et al. (2011)
13.	MIROC-ESM-CHEM	192 × 256 × 44	Watanabe et al. (2011)
14.	MRI-CGCM3	368 × 360 × 50	Yukimoto et al., 2012
15.	NorESM1-M	320 × 384 × 53	Iversen et al. (2013)

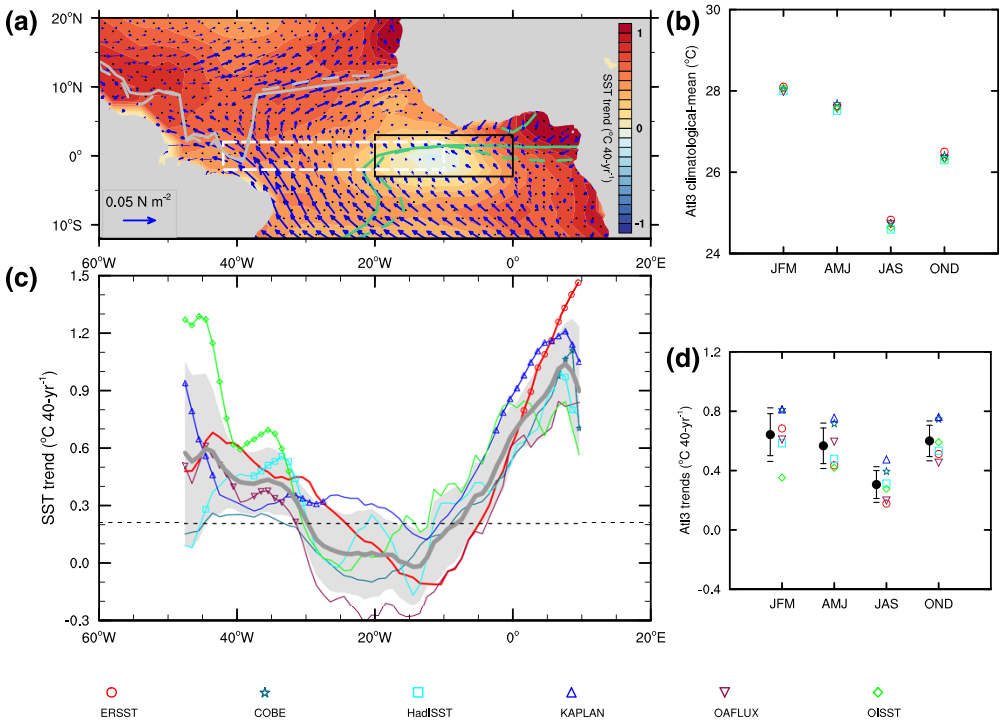

Figure 1. Warming hole in the equatorial Atlantic during 1979–2018. (a) Trends (calculated from ERSST) of the summer (JAS) SST (color scale; statistically significant values at the 95% confidence level are stippled) and surface wind stress from the bias-corrected TROPFLUX data set (thick vectors are statistically significant at the 95% confidence level). The solid box shows the Atl3 region: 3°S to 3°N, 0°–20°W; the dashed box shows the region over which wind stress discussed in section is averaged as defined by Bunge and Clarke (2009). The gray and green curves denote the climatological-mean ITCZ (defined as the latitude of zero meridional wind stress in the region 10°S to 20°N) and cold tongue edge (defined by a mean SST of 25 °C), respectively. To construct the solid curves, the 40-year trends have been removed from the JAS mean ITCZ and SST; the dashed curves include the 40-year trends. (b and d) Climatological mean and trends of the Atl3 index in observations. The vertical bars in (d) indicate the 90% and 95% confidence intervals using the six observational datasets. (c) Trends of zonally averaged SST across the equatorial Atlantic (3°S to 3°N) in different data sets; statistically significant trends are marked by unfilled shapes. The gray curve and filled area show the multi-data set mean and 95% confidence limit, respectively. The mean SST trend in the Atl3 region (0.21 °C) is shown using the dashed horizontal line.

0.2 ± 0.13 °C per 40 years in JAS). The mean ocean-atmosphere changes between these two seasons can be linked to a strengthening of the southeasterly trade winds and cold tongue development (Foltz et al., 2019; Lübbecke et al., 2018; Nnamchi et al., 2016; Okumura & Xie, 2004; Tokinaga & Xie, 2011; Xie & Carton, 2004).

Superimposed on the SST annual cycle, the SST trends imply an 11% increase of the annual cycle during 1979–2018, as measured by the change in seasonal cooling from AMJ to JAS. However, the cold tongue region has not increased in size or may have even shrunk slightly (the dashed green curve in Figure 1a), suggesting that the satellite era warming hole is a localized phenomenon. Thus, the present study focuses on the equatorial Atlantic Ocean. Further analyses are required to better understand the possible large-scale connections, but this is beyond the scope of the present study.

The trends in wind stress in Figure 1a correspond to a strengthening of the climatogical wind stress south of the equator and over the western equatorial Atlantic where wind changes are considered key to the tongue changes (Castaño-Tierno et al., 2018; Keenlyside & Latif, 2007; Martín-Rey & Lazar, 2019; Nnamchi et al., 2015; Pottapinjara et al., 2019; Richter et al., 2013; Zebiak, 1993). The wind stress changes point to an acceleration of the southeasterly trade winds (as discussed by Servain et al., 2014), although there are some uncertainties in the Atl3 region among the different reanalysis data sets (Figures 1a and 3).

Consistent with a previous study (Li et al., 2015), the tropical North Atlantic depicts prominent warming and a meridional gradient with increasing SST trends north of the equator (Figure 2). A meridional shift of the Intertropical Convergence Zone (ITCZ, shown by the dashed gray curve in Figure 1a) is not obvious despite a weakening of the northeasterly trade winds in parts of the basin giving rise to a characteristic "C-shape"

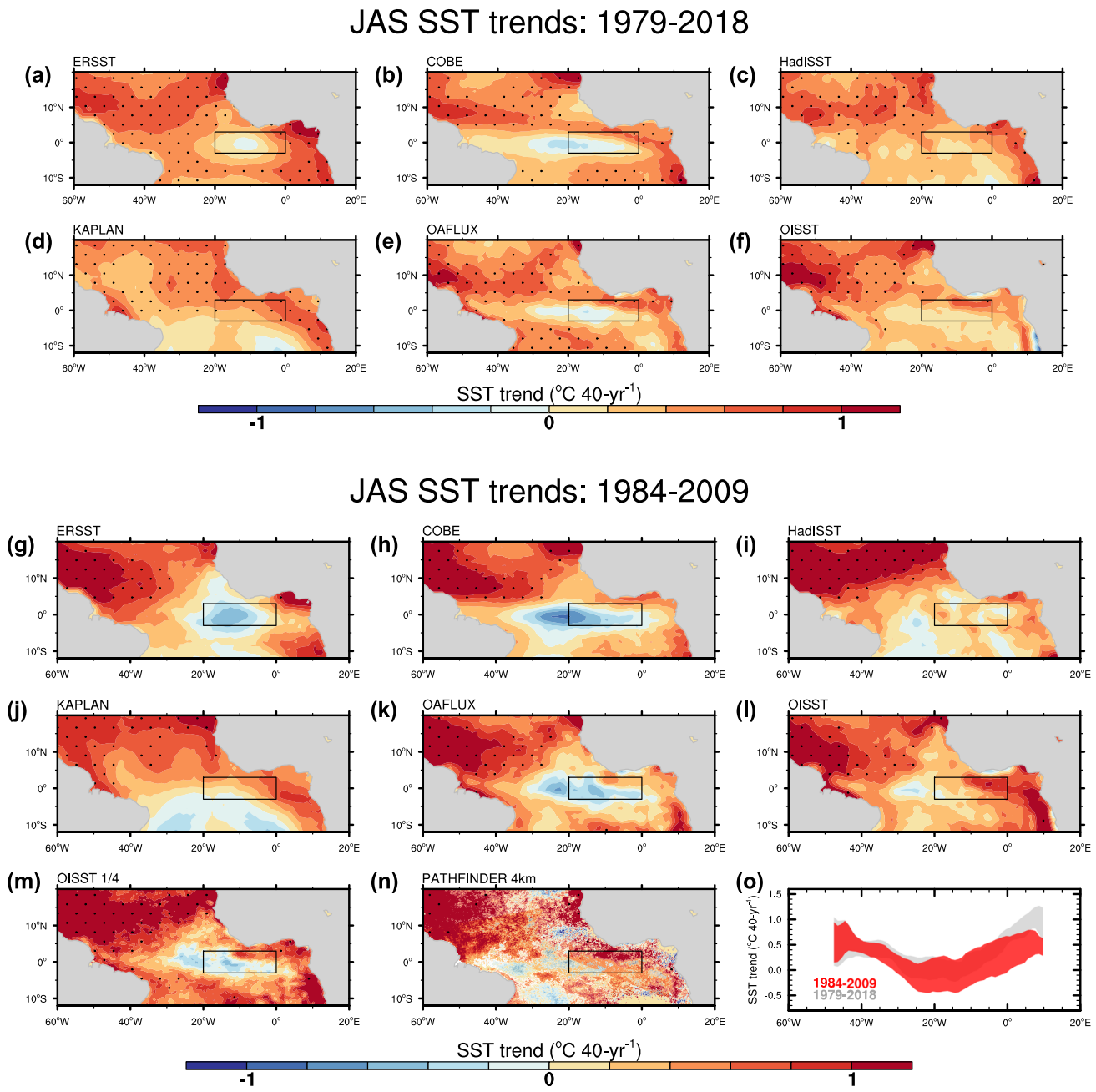

Figure 2. Spatial patterns of the warming hole in JAS using different data sets during (a–f) 1979–2018 (1982–2018 for the OISST in f) and (g–n) 1984–2009. The data sets are indicated on the top-left corner of each panel. The box shows the Atl3 region. (o) Trends of zonally averaged SST across the equatorial Atlantic (3°S to 3°N); the filled area shows 95% confidence limit based on 1984–2009 (red) and 1979–2018 (gray), respectively.

wind stress structure. At decadal time scales, this tropical Atlantic configuration has been linked to changes in the Atlantic Multidecadal Variability and the meridional overturning ocean circulation (Chang et al., 1997; Polo et al., 2013; Ruprich-Robert et al., 2017).

4. Surface Heat Flux and Ocean Circulation Changes

Local SST trends are governed by a combination of changes in net surface heat flux, Q_{net}, and ocean circulation effects. Here we analyze the OAFLUX data set that provides an observational estimate of the Q_{net} based on satellite-derived radiative fluxes (Rossow & Schiffer, 1999) and in situ-derived turbulent fluxes (Yu &

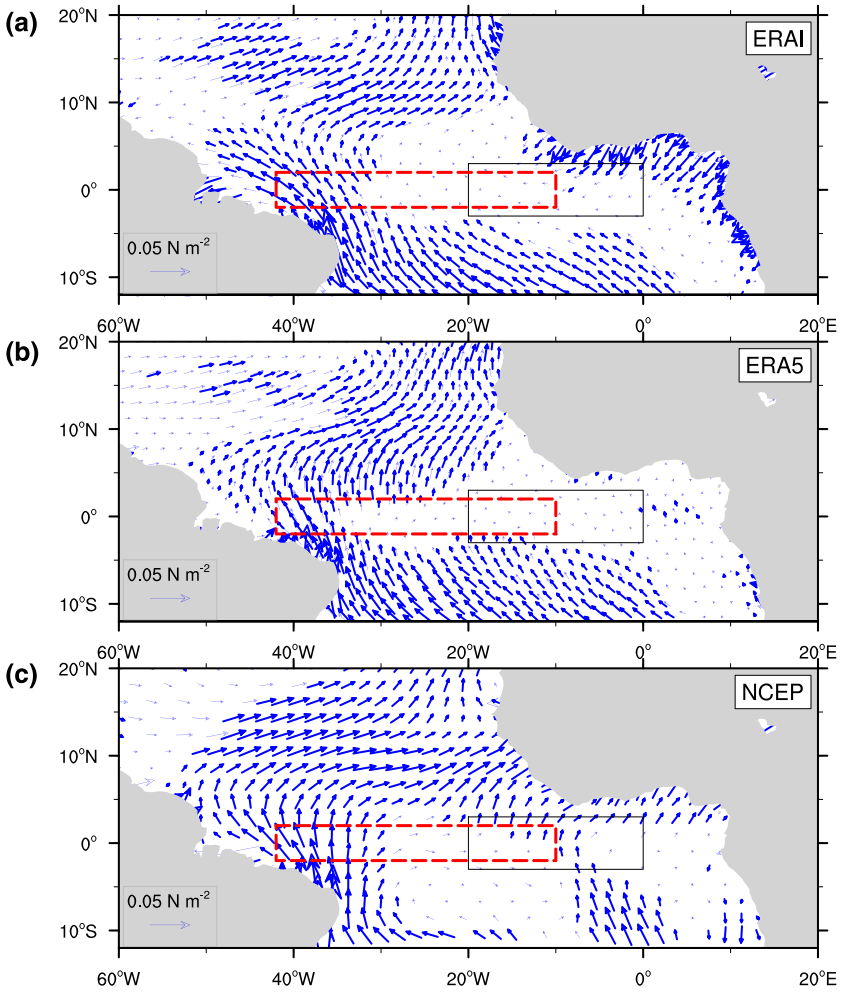

Figure 3. JAS trends of wind stress in ERAI, ERA5, and NCEP, 1979–2018. Thick vectors are statistically significant at the 95% confidence level. The data sets are indicated on the bottom-left corner of each panel.

Weller, 2007), and which is available for the period 1984–2009. As discussed in section 3, the warming hole is also pronounced during 1984–2009, and so we can investigate the possible roles of Q_{net} using this period. The OAFLUX Q_{net} and SST trend patterns are generally anticorrelated over the equatorial Atlantic Ocean (Figures 4). Positive Q_{net} trends indicate the ocean gains heat, and thus, this cannot explain the lack of SST warming. Despite the substantial differences among the patterns, they all show more heat entering the ocean in the region of cooling during this period.

The positive Q_{net} trends imply that the atmosphere damps the SST changes in the warming hole region. To better understand the damping mechanism, we decompose the Q_{net} into its radiative ($Q_{SW} + Q_{LW}$) and turbulent ($Q_{LH} + Q_{SH}$) components, where Q_{SW}, Q_{LW}, Q_{LH}, and Q_{SH} represent the shortwave, longwave, latent heat, and sensible heat fluxes, respectively. As shown in Figure 5, the radiative fluxes seem less important (Figures 5a–5e), the warming hole is primarily damped by the turbulent fluxes (Figures 5f–5j). The turbulent fluxes are controlled by the wind speed and air-sea humidity and temperature differences according to the bulk parameterizations:

$$Q_{LH} = -\rho L_e c_e U[q_s - q_a], \tag{1}$$

$$Q_{SH} = -\rho C_p c_h U[T_s - T_a], \tag{2}$$

where ρ is the surface air density; C_p is specific heat capacity at constant pressure and L_e is the latent heat of

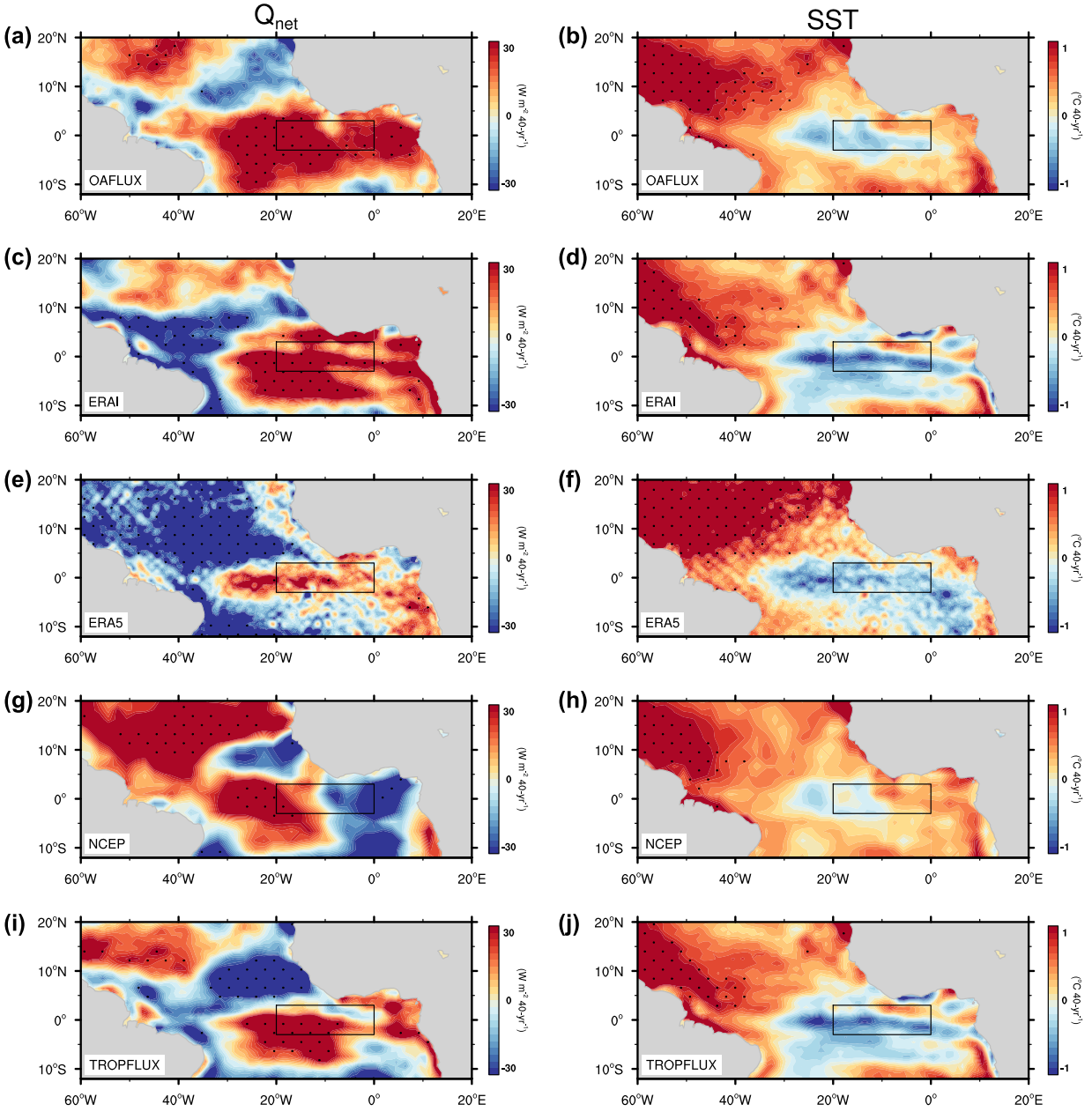

Figure 4. Trends of the Q_{net} trends and the corresponding SST trends, 1984–2009. Left panels: (a) the trends based on satellite-derived radiative fluxes (Rossow & Schiffer, 1999) and in situ derived turbulent fluxes (Yu & Weller, 2007). Positive flux trends indicate that the ocean gains heat from the atmosphere. The subsequent panels are Q_{net} based on the reanalysis data sets indicated on the bottom-left corner. Right panels: SST trends for the data sets shown on the left panels. The OAFLUX data set (Figure 2k) is shown here for reference. In all panels, statistically significant trends at the 95% confidence level are stippled.

vaporization; and c_e and c_h are the stability- and height-dependent turbulent exchange coefficients for latent and sensible heat. The term T_a denotes the temperature and q_a the specific humidity at the reference height of 2 m above the surface and q_s the saturation specific humidity at the surface temperature (SST, *T*s). The Q_{LH} typically dominates the turbulent fluxes over tropical oceans. The wind stress trends are quite uncertain over the warming hole (Figures 1a and 3). Assuming the winds were unchanged during the satellite era, the Q_{LH} trends would largely be explained by air-sea humidity differences.

As the atmosphere damps the SST changes over the warming hole, ocean dynamical processes must account for the lack of SST warming. The vertical profiles of ocean temperature across the equatorial Atlantic 3°S to 3°N depict cooling trends beneath the sea surface in all analyzed datasets (Figure 6). These are located near

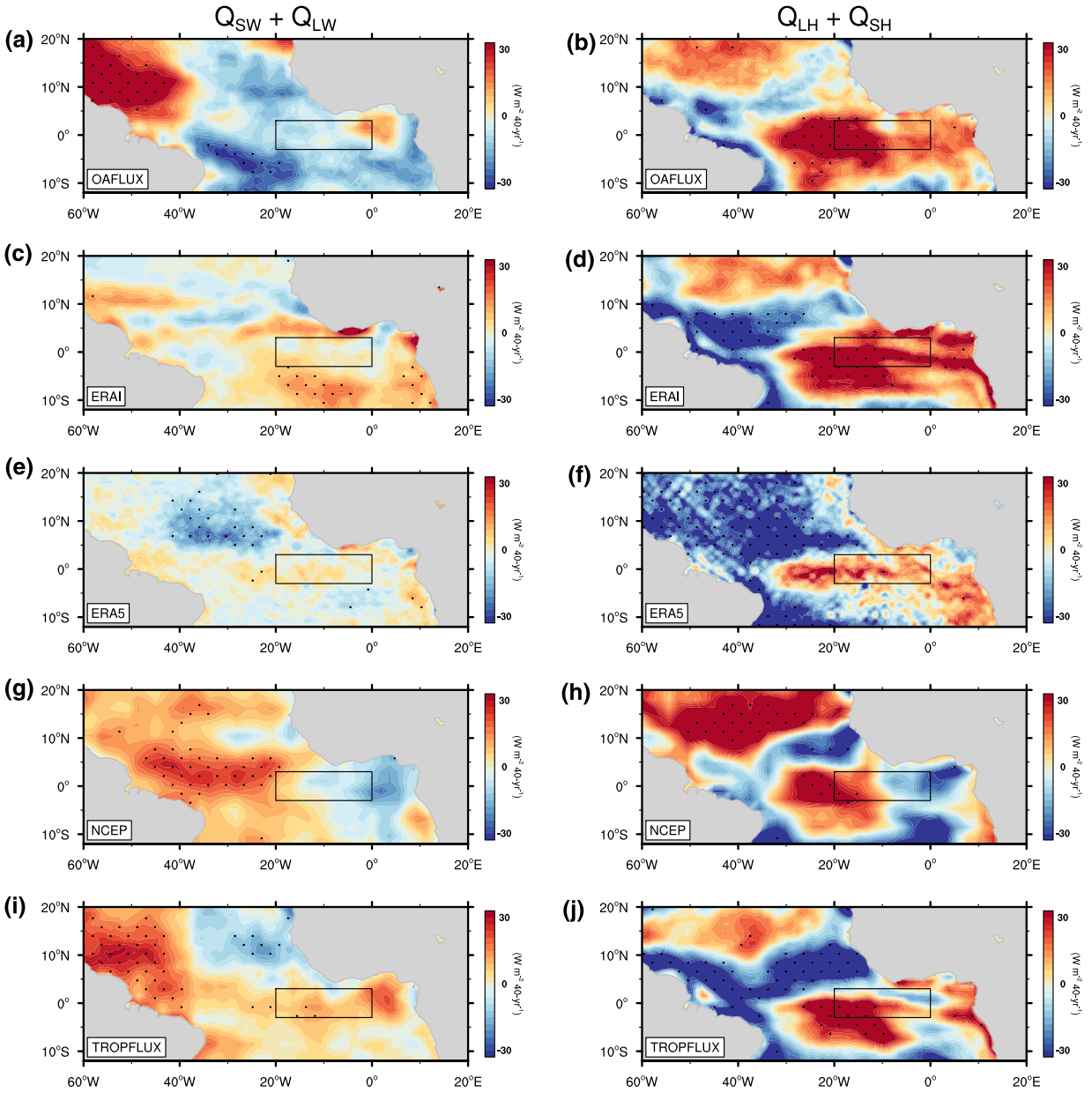

Figure 5. Decomposition of the Q_{net} into the radiative (left panels) and turbulent (right panels) components. Statistically significant trends at the 95% confidence level are stippled. The data sets are indicated on the bottom-left corner of each panel.

the thermocline defined by the 20 or 23 °C isotherm. There is, however, a large sensitivity of the position of the thermocline to the choice of data set, as exemplified by the differences between ORAS4 and ORAS5. Overall, the temperature profiles imply a shoaling of the equatorial thermocline, which would tend to cool the surface through climatological upwelling of anomalous cool subsurface temperature.

A thermocline shoaling can be caused by ocean dynamical processes through local and nonlocal wind stress forcing. The thermocline, defined as the depth of maximum vertical gradient of ocean temperature, is very sensitive to wind stress changes in the equatorial Atlantic (Castaño-Tierno et al., 2018). The wind changes over the western equatorial Atlantic are consistent with upwelling equatorial Kelvin wave that will cause a shoaling of the equatorial thermocline in the east (Ding et al., 2009). The zonal wind stress (τ_χ) averaged over the equatorial Atlantic exhibits a large annual cycle with a maximum during the boreal summer (Figure 7a). The $\tau_{\chi\ i}$ is averaged over the region 10–42°W, 2°S to 2°N shown in Figures 1 and 3. Locations

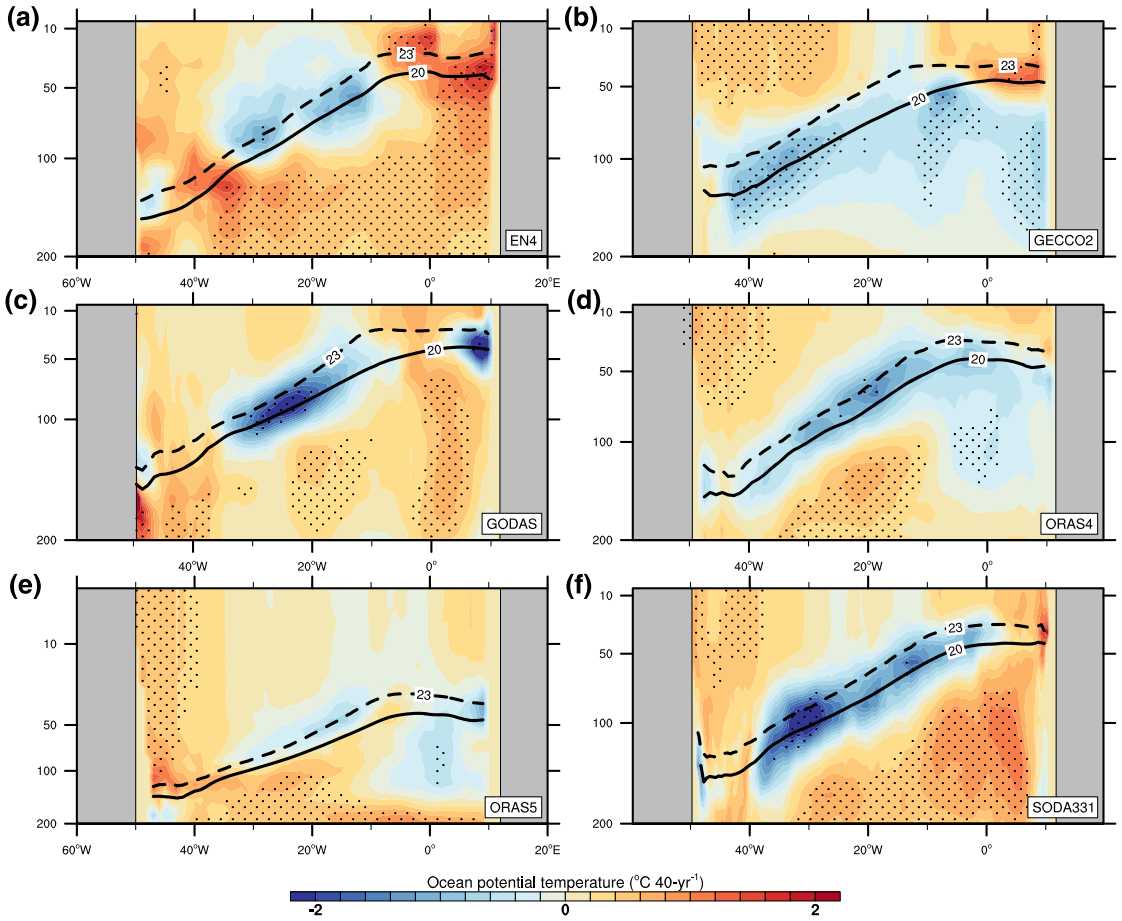

Figure 6. Vertical structure of the ocean temperature trends in JAS, 1979–2018. (a–f) The profile is based on the ocean potential temperature averaged in the equatorial Atlantic 3°S to 3°N using (a) in situ derived and (b–f) ocean reanalysis data sets. The curves show the climatological-mean 20 and 23 °C contours representing commonly used definitions of the thermocline. In all panels, stippling denotes statistically significant trends at the 95% confidence level.

east and west of this region are greatly affected by the African continent and mesoscale eddies, respectively (Bunge & Clarke, 2009), and are therefore not included in our analysis.

The τ_x in summer in all analyzed data sets shows strong trends that represent a strengthening of the prevailing easterlies (Figure 7b). The strong τ_x forcing is consistent with eastward shoaling of the thermocline suggested by the temperature profiles (Figure 6). This mechanisms is important for the annual cycle (Bunge & Clarke, 2009; Ding et al., 2009) and may explain why the warming deficit is most pronounced during the summer upwelling season. On the other hand, strong SST warming is observed to the east of the warming hole, where the prevailing winds are greatly modified by the African continent giving rise to a distinct variability (Bunge & Clarke, 2009; Li & Philander, 1997).

5. The Relative Roles of Intrinsic Variability and External Forcing

We discuss the possible roles of external forcing (GHGs and aerosols) and internal variability for the emergence of the warming hole in the equatorial Atlantic during the satellite era using the CMIP5 ensembles. The forced experiments end in 2005, and we analyze the CMIP5 ensembles and compare them with observations for the overlapping 27-year period from 1979 to 2005. The spread of the trends across the 15 models reflects both internal variability and model uncertainty, and the ensemble mean provides an estimate of the trend due to the prescribed external forcing.

The “all forcing” ensemble, representing the combined effects of GHGs and aerosols, significantly overestimates the observed satellite era Atl3 SST trends (Figures 8a and 9b). The CMIP models exhibit systematic

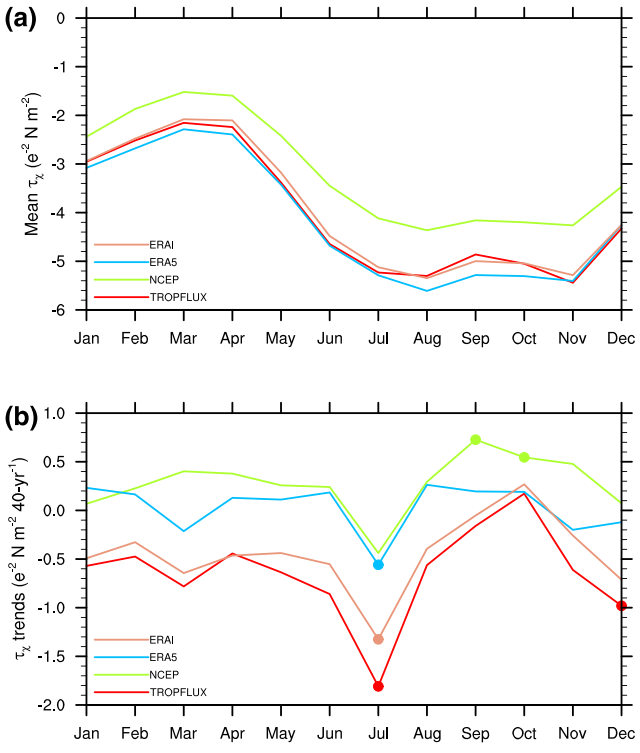

Figure 7. Seasonality of wind stress over the equatorial Atlantic, 1979–2018. Shown are the (a) mean and (b) trends of the τ_x averaged over the region 10–42°W, 2°S to 2°N (shown in Figures 1 and 3) as defined by Bunge and Clarke (2009). Negative (positive) τ_x values denote easterlies (westerlies). In (b), filled circular ticks denote statistical significance at the 95% confidence level.

biases in the mean-state SST (Prodhomme et al., 2019; Richter et al., 2014; Richter & Xie, 2008; Wang et al., 2014), but we do not find any clear relationship of the SST trends to model biases. The strong overestimation of the SST trends could argue for internal variability as the source of the warming hole. Greenhouse gas forcing dominates the warming trends over the cold tongue (Figures 8a and 9c). In contrast, the aerosol-forced ensemble hardly depicts significant trends in the Atl3 region (Figures 8a and 9d). However, there are strong SST trends north of the equator (Figure 9d), consistent with decreased atmospheric aerosol loading over North Atlantic in recent decades (Booth et al., 2012).

The role of aerosols in Atlantic climate variability is a contentious subject of ongoing research (Bellomo et al., 2017; Booth et al., 2012; Evan et al., 2009; Haustein et al., 2019; Yan et al., 2019; Zhang et al., 2013). Previous studies discussed interhemispheric SST gradient over tropical Atlantic (with warmer south and colder north) as robust response to aerosol forcing in climate models during the twentieth century (Biasutti & Giannini, 2006; Booth et al., 2012; Chang et al., 2011; Held et al., 2005). The analysis here also shows ensemble SST trends that are consistent with aerosol forcing during the satellite era. However, the large differences between the ensemble-SST trends simulated in the "all forcing" experiment, and observations highlight the difficulty in understanding the roles of external forcing, as the role of aerosols may be underestimated in the models.

The observed interannual variability in equatorial Atlantic, represented by standard deviation of the Atl3 index, amounts to 0.4 °C (Figure 8b). This is closely reproduced in all CMIP5 ensembles. However, the standard deviations in the models are not obviously related to the simulated Atl3 trends.

To estimate the trend for the piControl ensemble, we first create similar 27-year (k) chunks using 300-year of integration integration (n) of each model. Thus, there are n–k or 273 chunks leading to 273 SST trend maps for each model. The multimodel mean and standard deviation of the trend maps are calculated (Figures 9e and 9f). As expected, the unforced piControl ensemble, which only provides the internal variability of the coupled models, exhibits zero trends over the equatorial Atlantic in the ensemble mean (Figure 9e). The internal variability estimated by the multimodel standard deviation, which has been multiplied by −1 to facilitate comparison with the observed cooling trend, exhibits strong SST cooling trends (Figures 8a and 9f). The internal variability, as represented by the standard deviation of the piControl ensemble SST trends, can potentially cool temporarily the Atl3 region beyond the 95% limit of the greenhouse gas and aerosol effects 1979–2005 (Figure 8a).

We further illustrate the possible roles of internal variability by placing the recent warming hole in a historical observational context using the JAS Atl3 40-year running trend 1870–2018 (Figure 10). The choice of 40-year windows aims to clarify whether or not the 1979–2018 equatorial Atlantic warming hole is unusual during the twentieth century. The 40-year running-trend curve exhibits multidecadal fluctuations; weak SST trends were also observed during the 1890s–1910s and 1940s–1960s, accompanied by epochs of stronger trends. These previous weak trends suggest that the satellite era warming hole is not unusual during the twentieth century.

The Atl3 running-trend curves in the different data sets exhibit an overall statistically significant upward trend of 0.25 ± 13 °C per 40 years. By removing this long-term trend that can be largely attributable to external forcing, which dominates trends in the climate system (Stocker et al., 2013), multidecadal fluctuations emerge that may reflect internal variability (dashed red curves in Figure 10). Based on the detrended curves, there are large changes in the magnitude of the running trends and in timing of the phase shift. The recent warming hole starts earlier, and the 1979–2018 trend drops from 0.44 ± 0.16 °C per 40 years to −0.16 ± 0.34 °C per 40 years based on the detrended curves. Thus, external forcing may have contributed

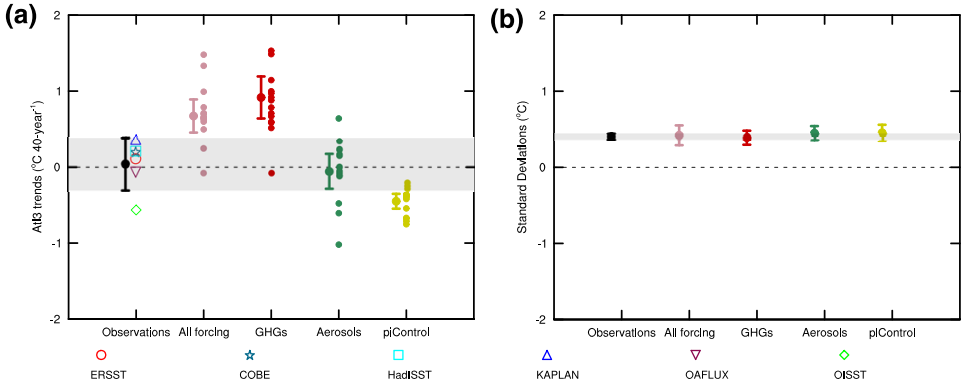

Figure 8. Internal and external forcing of the equatorial Atlantic SST trends. (a) JAS Atl3 SST trends in observations and externally forced historical experiments (all forcing, GHGs, and aerosols) 1979–2005 and 300-year run of the unforced piControl. For the piControl, the trends were first estimated using similar (27-year) chunks and then the standard deviation of the trends estimated and inverted for plotting. (b) Interannual variability of the Atl3 index in the CMIP5 ensemble. The index is for JAS during 1979–2005 in observations and externally forced historical experiments (all forcing, GHGs, and aerosols); for the unforced piControl, 300-year of integration was analyzed. Note that the two panels are based on the same scale to facilitate immediate visual comparison.

about 0.60 °C per 40 years warming of the cold tongue during the recent period, without which the satellite era warming hole would have been substantially colder. Thus, although the warming hole may be internally driven, the SST trends appear to have been strongly modulated by external forcing.

Previous studies show that the internal low-frequency variability superposes strongly the global warming effects during the recent decades (Dong & Zhou, 2014; Liu & Sui, 2014). The satellite era Atlantic trends are characterized by a conspicuous cross-equatorial gradient with warmer Northern Hemisphere and cooler Southern Hemisphere with respect to the SST and subsurface ocean temperatures, implying regional

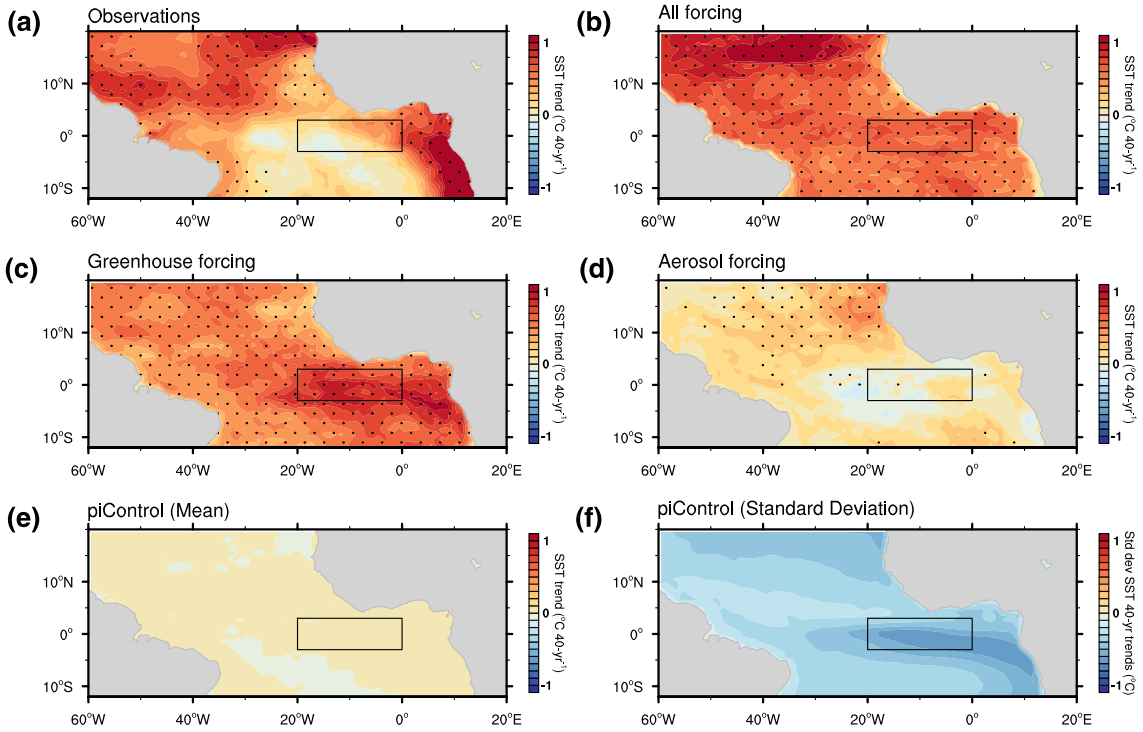

Figure 9. Mean trends of the observational and CMIP5 ensembles, 1979–2005. In (a)–(d), stippling denotes statistically significant trends at the 95% confidence level. For the unforced piControl, first, the trends were estimated using similar (27-year) chunks and then the (e) mean and (f) standard deviation of the trends estimated. Note that the standard deviation is inverted for plotting to be consistent with warming hole.

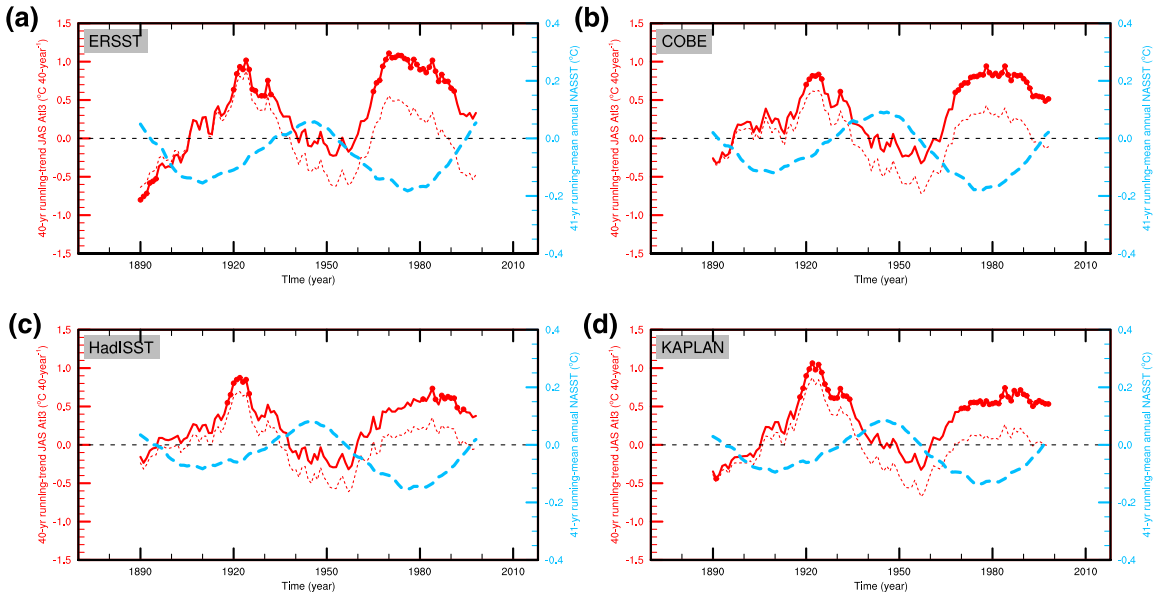

Figure 10. The 40-year running-trend of the Atl3 (red, the thin dashed curve has been detrended) and 41-year running-mean annual NASST index (dashed, blue) in the different data sets indicated on the top-left corner of each panel. The NASST is defined as Atlantic SST averaged from 0°N to 70°N, which has been detrended. Both curves are centered in time around the years indicated on the abscissa. For the Atl3 40-year trends, ticks denote statistical significance at the 95% confidence level.

changes in ocean heat content (Liu & Sui, 2014; Dong & Zhou, 2014; Li et al., 2014, 2015). The North Atlantic SST averaged from 0°N to 70°N (NASST) variability strengthened overall since the 1970s (Frajka-Williams et al., 2017) when the warming deficit emerged in the equatorial cold tongue region. Thus, the detrended 41-year low-pass filtered annual-mean NASST index shows an out-of-phase relationship with the Atl3 40-year running trend curve (Figure 10). The correlation between the two time series, a measure of the low-frequency behavior of the cross-equatorial SST gradient, is -0.57 ± 0.14 (using the nonparametric Spearman's rank correlation, significant at the 95% confidence level). Thus, there is a robust inverse relationship between the Atl3 SST trend changes and low-frequency NASST anomalies during the twentieth century.

6. Concluding Remarks

Although there has been a substantial warming of the tropical Atlantic (Deser et al., 2010; Li et al., 2014, 2015; Servain et al., 2014; Tokinaga & Xie, 2011), we uncover a warming hole during the satellite era, defined by small SST trends in the equatorial cold tongue region during the boreal summer upwelling season. Similar weak trends were also observed during the 1890s–1910s and 1940s–1960s, accompanied by epochs of strong trends. Thus, the satellite era warming hole in the equatorial Atlantic is not unusual during the twentieth century. The warming deficit appears to be driven by a shoaling of the equatorial thermocline and damped by the surface turbulent heat fluxes.

The satellite era warming hole in the equatorial Atlantic is associated with increased NASST anomalies and a cross-equatorial SST gradient. The low-frequency behavior of the NASST has been linked to the variability in ocean circulation (Gulev et al., 2013; McCarthy et al., 2015), surface fluxes (Clement et al., 2015; Keenlyside et al., 2015), and external forcing (Bellomo et al., 2017; Booth et al., 2012; Haustein et al., 2019). It is also strongly related to low-frequency variability over the Pacific (Kucharski et al., 2016; Sun et al., 2017; Zhang & Delworth, 2007).

An ensemble of 15 CMIP5 models show that greenhouse forcing warmed the cold tongue whereas aerosols cooled it during the satellite era. The combined effects of greenhouse and aerosol forcing grossly overestimate the equatorial Atlantic SST trends in the CMIP5 ensemble. Similarly, twentieth-century observations show that the SST trends would be of the order of about 0.60 °C per 40 years colder without the long-term monotonic trends, which may largely denote external forcing effects. Indeed, the CMIP5 ensemble shows

that the warming hole can potentially originate from internal variability of the climate system, as even larger cooling trends are present in the piControl experiment (Taylor et al., 2012). Thus, the satellite era warming hole reflects the interactions of internal variability with externally driven changes in the equatorial Atlantic. However, the understanding of the relative importance of internal variability and external forcing is hampered by uncertainties in observations and coupled models.

The interannual climate variability over the equatorial Atlantic has weakened during the recent decades (Tokinaga & Xie, 2011; Prigent et al., 2020). However, it remains unclear how the warming hole is related to changes in interannual variability, including fluctuations in the SST variance and spatial structure (Martín-Rey et al., 2018, 2019). More research is needed to better understand how the reversal of the previous oceanic warming in the North Atlantic since the mid-2000s (Robson et al., 2016) is related to the satellite era equatorial Atlantic.

Acknowledgments
This work was supported by the BANINO project of the German Ministry of Education and Research (BMBF). H. C. N. was funded by the Alexander von Humboldt Postdoctoral Fellowship. N. S. K. acknowledges support from EU H2020 programme (STERCP, grant 648982; TRIATLAS, grant 817578). The helpful comments from anonymous reviewers are greatly acknowledged. The data sets and CMIP5 model outputs were all taken from published sources indicated in Tables 11 and 22, respectively. The CMIP5 outputs are available online (https://pcmdi.llnl.gov/mips/cmip5/). The surface and ocean profile data sets were taken from the following publicly available sources (ERSST: https://www.esrl.noaa.gov/psd/data/gridded/data.noaa.ersst.v5.html, COBE: https://www.esrl.noaa.gov/psd/data/gridded/data.cobe2.html, HadISST: https://www.metoffice.gov.uk/hadobs/hadisst/, KAPLAN: https://www.esrl.noaa.gov/psd/data/gridded/data.kaplan_sst.html, OISST1° × 1°: https://www.esrl.noaa.gov/psd/data/gridded/data.noaa.oisst.v2.html, OISST¼°: https://www.esrl.noaa.gov/psd/data/gridded/data.noaa.oisst.v2.highres.html, NCEP: https://www.esrl.noaa.gov/psd/data/gridded/data.ncep.reanalysis.html, ERAI: https://www.ecmwf.int/en/forecasts/datasets/reanalysis-datasets/era-interim, ERA5: https://www.ecmwf.int/en/forecasts/datasets/reanalysis-datasets/era5, PATHFINDER: https://www.nodc.noaa.gov/SatelliteData/pathfinder4km/, TROPFLUX: https://incois.gov.in/tropflux/, EN4:https://www.metoffice.gov.uk/hadobs/en4/, GECCO2: https://icdc.cen.uni-hamburg.de/1/daten/reanalysis-ocean/gecco2.html, GODAS: https://www.esrl.noaa.gov/psd/data/gridded/data.godas.html, ORAS4: http://icdc.cen.uni-hamburg.de/projekte/easy-init/easy-init-ocean.html, ORAS5: http://icdc.cen.uni-hamburg.de/projekte/easy-init/easy-init-ocean.html, and SODA331: http://apdrc.soest.hawaii.edu/dods/public_data/SODA/soda_3.3.1).

References

Arora, V. K., Scinocca, J. F., Boer, G. J., Christian, J. R., Denman, K. L., Flato, G. M., et al. (2011). Carbon emission limits required to satisfy future representative concentration pathways of greenhouse gases. *Geophysical Research Letters*, *38*, L05805. https://doi.org/10.1029/2010GL046270

Balmaseda, M. A., Mogensen, K., & Weaver, A. T. (2013). Evaluation of the ECMWF ocean reanalysis system ORAS4. *Quarterly Journal of the Royal Meteorological Society*, *139*, 1132–1161. https://doi.org/10.1002/qj.2063

Behringer, D. W., Ji, M., & Leetmaa, A. (1998). An improved coupled model for ENSO prediction and implications for ocean initialization. Part I: The ocean data assimilation system. *Monthly Weather Review*, *126*, 1013–1021. https://doi.org/10.1175/1520-0493(1998)126<1013:AIC

Bellomo, K., Murphy, L., Cane, M., Clement, A., & Polvani, L. (2017). Historical forcings as main drivers of the Atlantic multidecadal variability in the CESM large ensemble. *Climate Dynamics*, *50*(9–10), 3687–3698. https://doi.org/10.1007/s00382-017-3834-3

Biasutti, M., & Giannini, A. (2006). Robust Sahel drying in response to late 20th century forcings. *Geophysical Research Letters*, *33*, L11706. https://doi.org/10.1029/2006GL026067

Bindoff, N. L., Stott, P. A., AchutaRao, K. M., Allen, M. R., Gillett, N., Gutzler, D., et al. (2013). Detection and Attribution of Climate Change: From Global to Regional. In T. F. Stocker, D. Qin, G.-K. Plattner, M. Tignor, S. K. Allen, J. Boschung, et al. (Eds.), *Climate Change 2013: The Physical Science Basis. Contribution of Working Group I to the Fifth Assessment Report of the Intergovernmental Panel on Climate Change* (Chap. 2, pp. 159–254). Cambridge, United Kingdom and New York, NY, USA: Cambridge University Press.

Booth, B. B., Dunstone, N. J., Halloran, P. R., Andrews, T., & Bellouin, N. (2012). Aerosols implicated as a prime driver of twentieth-century North Atlantic climate variability. *Nature*, *484*(7393), 228–232. https://doi.org/10.1038/nature10946

Bunge, L., & Clarke, A. (2009). Seasonal propagation of sea level along the equator in the Atlantic. *Journal of Physical Oceanography*, *39*(4), 1069–1074. https://doi.org/10.1175/2008jpo4003.1

Caesar, L., Rahmstorf, S., Robinson, A., Feulner, G., & Saba, V. (2018). Observed fingerprint of a weakening Atlantic Ocean overturning circulation. *Nature*, *556*, 191–196. https://doi.org/10.1038/s41586-018-0006-5

Carton, J. A., Chepurin, G. A., & Chen, L. (2018). SODA3: A new ocean climate reanalysis. *Journal of Climate*, *31*, 6967–6983. https://doi.org/10.1175/JCLI-D-18-0149.1

Castaño-Tierno, A., Mohino, E., Rodríguez-Fonseca, B., & Losada, T. (2018). Revisiting the CMIP5 thermocline in the equatorial Pacific and Atlantic oceans. *Geophysical Research Letters*, *45*, 12,963–12,971. https://doi.org/10.1029/2018GL079847

Chang, C., Chiang, J., Wehner, M., Friedman, A., & Ruedy, R. (2011). Sulfate aerosol control of tropical Atlantic climate over the twentieth century. *Journal of Climate*, *24*(10), 2540–2555. https://doi.org/10.1175/2010jcli4065.1

Chang, P., Ji, L., & Li, H. (1997). A decadal climate variation in the tropical Atlantic Ocean from thermodynamic air-sea interactions. *Nature*, *385*, 516–518. https://doi.org/10.1038/385516a0

Clement, A., Bellomo, K., Murphy, L. N., Cane, M. A., Mauritsen, T., Radel, G., & Stevens, B. (2015). The Atlantic Multidecadal Oscillation without a role for ocean circulation. *Science*, *350*(6258), 320–324. https://doi.org/10.1126/science.aab3980

Collins, W. J., Bellouin, N., Doutriaux-Boucher, M., Gedney, N., Halloran, P., Hinton, T., et al. (2011). Development and evaluation of an Earth-System model—HadGEM2. *Geoscientific Model Development*, *4*(4), 1051–1075. https://doi.org/10.5194/gmd-4-1051-2011

Dee, D. P., Uppala, S. M., Simmons, A. J., Berrisford, P., Poli, P., Kobayashi, S., et al. (2011). The ERA-interim reanalysis: Configuration and performance of the data assimilation system. *Quarterly Journal of the Royal Meteorological Society*, *137*(656), 553–597. https://doi.org/10.1002/qj.828

Delworth, T. L., Broccoli, A. J., Rosati, A., Stouffer, R. J., Balaji, V., Beesley, J. A., et al. (2006). GFDL's CM2 global coupled climate models. Part I: Formulation and simulation characteristics. *Journal of Climate*, *19*(5), 643–674. https://doi.org/10.1175/JCLI3629.1

Deser, C., Phillips, A. S., & Alexander, M. A. (2010). Twentieth century tropical sea surface temperature trends revisited. *Geophysical Research Letters*, *37*, L10701. https://doi.org/10.1029/2010GL043321

Ding, H., Keenlyside, N., & Latif, M. (2009). Seasonal cycle in the upper equatorial Atlantic Ocean. *Journal of Geophysical Research*, *114*, C09016. https://doi.org/10.1029/2009JC005418

Dong, L., & Zhou, T. (2014). The formation of the recent cooling in the Eastern Tropical Pacific Ocean and the associated climate impacts: A competition of global warming, IPO, and AMO. *Journal of Geophysical Research-Atmospheres*, *119*, 11,272–11,287. https://doi.org/10.1002/2013JD021395

Drijfhout, S., van Oldenborgh, G. J., & Cimatoribus, A. (2012). Is a decline of AMOC causing the warming hole above the North Atlantic in observed and modeled warming patterns? *Journal of Climate*, *25*, 8373–8379. https://doi.org/10.1175/JCLI-D-12-00490.1

Dufresne, J.-L., Foujols, M. A., Denvil, S., Caubel, A., Marti, O., Aumont, O., et al. (2013). Climate change projections using the IPSL-CM5 Earth system model: From CMIP3 to CMIP5. *Climate Dynamics*, *40*(9-10), 2123–2165. https://doi.org/10.1007/s00382-012-1636-1

Dunne, J. P., John, J. G., Shevliakova, E., Stouffer, R. J., Krasting, J. P., Malyshev, S. L., et al. (2012). GFDL's ESM 2 global coupled climate-carbon Earth system models. Part I: Physical formulation and baseline simulation characteristics. *Journal of Climate*, *25*, 6646–6665. https://doi.org/10.1175/JCLI-D-11-00560.1

Evan, A. T., Vimont, D. J., Heidinger, A. K., Kossin, J. P., & Bennartz, R. (2009). The role of aerosols in the evolution of tropical North Atlantic Ocean temperature anomalies. *Science*, *324*(5928), 778–781. https://doi.org/10.1126/science.1167404

Foltz, G. R., Brandt, P., Richter, I., Rodríguez-Fonseca, B., Hernandez, F., Dengler, M., et al. (2019). The tropical Atlantic observing system. *Frontiers in Marine Science*, *6*. https://doi.org/10.3389/fmars.2019.00206

Frajka-Williams, E., Beaulieu, C., & Duchez, A. (2017). Emerging negative Atlantic multidecadal oscillation index in spite of warm subtropics. *Scientific Reports*, *7*, 11224. https://doi.org/10.1038/s41598-017-11046

Gent, P. R., Danabasoglu, G., Donner, L. J., Holland, M. M., Hunke, E. C., Jayne, S. R., et al. (2011). The community climate system model version 4. *Journal of Climate*, *24*(19), 4973–4991. https://doi.org/10.1175/2011JCLI4083.1

Gervais, M., Shaman, J., & Kushnir, Y. (2018). Mechanisms governing the development of the North Atlantic warming hole in the CESM-LE future climate simulations. *Journal of Climate*, *31*(15), 5927–5946. https://doi.org/10.1175/jcli-d-17-0635.1

Good, S. A., Martin, M. J., & Rayner, N. A. (2013). EN4: Quality controlled ocean temperature and salinity profiles and monthly objective analyses with uncertainty estimates. *Journal of Geophysical Research, Oceans*, *118*, 6704–6716. https://doi.org/10.1002/2013JC009067

Gulev, S. K., Latif, M., Keenlyside, N., Park, W., & Koltermann, K. P. (2013). North Atlantic Ocean control on surface heat flux at multidecadal timescales. *Nature*, *499*(7459), 464–467. https://doi.org/10.1038/nature12268

Haarsma, R. J., Campos, E., Hazeleger, W., & Severijns, C. (2008). Influence of the Meridional overturning circulation on tropical Atlantic climate and variability. *Journal of Climate*, *21*, 1403–1416. https://doi.org/10.1175/2007JCLI1930.1

Haustein, K., Otto, F. E., Venema, V., Jacobs, P., Cowtan, K., Hausfather, Z., et al. (2019). A limited role for unforced internal variability in twentieth-century warming. *Journal of Climate*, *32*, 4893–4917. https://doi.org/10.1175/JCLI-D-18-0555.1

Held, I. M., Delworth, T. L., Lu, J., Findell, K. L., & Knutson, T. R. (2005). Simulation of Sahel drought in the 20th and 21st centuries. *Proceedings of the National Academies of Sciences of the United States of America*, *102*, 17,891–17,896. https://doi.org/10.1073/pnas.0509057102

Hersbach, H., de Rosnay, P., Bell, B., Schepers, D., Simmons, A., Soci, C., et al. (2018). Operational global reanalysis: Progress, future directions and synergies with NWP. ERA Report Series. doi.https://doi.org/10.21957/tkic6g3wm

Hirahara, S., Ishii, M., & Fukuda, Y. (2014). Centennial-scale sea surface temperature analysis and its uncertainty. *Journal of Climate*, *27*, 57–75. https://doi.org/10.1175/JCLI-D-12-00837.1

Huang, B., Thorne, P. W., Banzon, V. F., Boyer, T., Chepurin, G., Lawrimore, J. H., et al. (2017). Extended Reconstructed Sea Surface Temperature, Version 5 (ERSSTv5): Upgrades, validations, and intercomparisons. *Journal of Climate*, *30*(20), 8179–8205. https://doi.org/10.1175/JCLI-D-16-0836.1

Iversen, T., Bentsen, M., Bethke, I., Debernard, J. B., Kirkevåg, A., Seland, Ø., et al. (2013). The Norwegian Earth System Model, NorESM1–M. Part 2: Climate response and scenario projections. *Geoscientific Model Development*, *6*(2), 389–415. https://doi.org/10.5194/gmd-6-389-2013

Kalnay, E., Kanamitsu, M., Kistler, R., Collins, W., Deaven, D., Gandin, L., et al. (1996). The NCEP/NCAR 40-year reanalysis project. *Bulletin of the American Meteorological Society*, *77*(3), 437–471. https://doi.org/10.1175/1520-0477(1996)077<0437:TNYRP>2.0.CO;2

Kaplan, A., Cane, M. A., Kushnir, Y., Clement, A. C., Blumenthal, M. B., & Rajagopalan, B. (1998). Analyses of global sea surface temperature 1856–1991. *Journal of Geophysical Research*, *103*(C9), 18567–18589. https://doi.org/10.1029/97JC01736

Keenlyside, N. S., Ba, J., Mecking, J., Omrani, N. E., Latif, M., Zhang, R., & Msadek, R. (2015). North Atlantic multi-decadal variability—Mechanisms and predictability. In C.-P. Chang, M. Ghil, M. Latif, & M. Wallace (Eds.), *Climate Change: Multidecadal and Beyond* (Chap. 9, pp. 141–157). Singapore, ISBN 978-9814579926: World Scientific Publishing Company. https://doi.org/10.1142/9789814579933_0009

Keenlyside, N. S., & Latif, M. (2007). Understanding equatorial Atlantic interannual variability. *Journal of Climate*, *20*, 131–142. https://doi.org/10.1175/JCLI3992.1

Kendall, M. G. (1975). *Rank Correlation Methods* (4th ed.). London: Charles Griffin.

Kilpatrick, K. A., Podestá, G. P., & Evans, R. (2001). Overview of the NOAA/NASA advanced very high resolution radiometer Pathfinder algorithm for sea surface temperature and associated matchup database. *Journal of Geophysical Research*, *106*(C5), 9179–9197. https://doi.org/10.1029/1999JC000065

Köhl, A. (2015). Evaluation of the GECCO2 ocean synthesis: Transports of volume, heat and freshwater in the Atlantic. *Quarterly Journal of the Royal Meteorological Society*, *141*, 166–181. https://doi.org/10.1002/qj.2347

Kucharski, F., Ikram, F., Molteni, F., Farneti, R., Kang, I. S., No, H. H., et al. (2016). Atlantic forcing of Pacific decadal variability. *Climate Dynamics*, *46*(7-8), 2337–2351. https://doi.org/10.1007/s00382-015-2705-z

Kumar, B. P., Vialard, J., Lengaigne, M., Murty, V., & McPhaden, M. (2012). TropFlux: Air-sea fluxes for the global tropical oceans-description and evaluation. *Climate Dynamics*, *38*, 1521–1543. https://doi.org/10.1007/s00382-011-1115-0

Li, T., & Philander, S. (1997). On the seasonal cycle of the equatorial Atlantic Ocean. *Journal of Climate*, *10*(4), 813–817. https://doi.org/10.1175/1520-0442(1997)010<0813:otscot>2.0.co;2

Li, X., Xie, S.-P., Gille, S. T., & Yoo, C. (2015). Atlantic-induced pan-tropical climate change over the past three decades. *Nature Climate Change*, *6*, 275–279. https://doi.org/10.1038/nclimate2840

Li, X. C., Holland, D. M., Gerber, E. P., & Yoo, C. (2014). Impacts of the north and tropical Atlantic Ocean on the Antarctic Peninsula and sea ice. *Nature*, *505*(7484), 538–542. https://doi.org/10.1038/nature12945

Liu, P., & Sui, C. A. H. (2014). An observational analysis of the oceanic and atmospheric structure of global scale multidecadal variability. *Advances in Atmospheric Sciences*, *31*(2), 316–330. https://doi.org/10.1007/s00376-013-2305-y

Lübbecke, J. F., Rodríguez-Fonseca, B., Richter, I., Martín-Rey, M., Losada, T., Polo, I., & Keenlyside, N. S. (2018). Equatorial Atlantic variability—Modes, mechanisms, and global teleconnections. *WIREs Climate Change*, *9*(4), e527. https://doi.org/10.1002/wcc.527

Mann, H. B. (1945). Non-parametric tests against trend. *Econometrica*, *13*, 245–259.

Martín-Rey, M., & Lazar, A. (2019). Is the boreal spring tropical Atlantic variability a precursor of the equatorial mode? *Climate Dynamics*, *53*(3-4), 2339–2353. https://doi.org/10.1007/s00382-019-04851-9

Martín-Rey, M., Polo, I., Rodríguez-Fonseca, B., Lazar, A., & Losada, T. (2019). Ocean dynamics shapes the structure and timing of Atlantic equatorial modes. *Journal of Geophysical Research, Oceans*, *124*, 7529–7544. https://doi.org/10.1029/2019JC015030

Martín-Rey, M., Polo, I., Rodríguez-Fonseca, B., Losada, T., & Lazar, A. (2018). Is there evidence of changes in tropical Atlantic variability modes under AMO phases in the observational record? *Journal of Climate*, *31*, 515–536. https://doi.org/10.1175/JCLI-D-16-0459.1

McCarthy, G. D., Haigh, I. D., Hirschi, J. J.-M., Grist, J. P., & Smeed, D. A. (2015). Ocean impact on decadal Atlantic climate variability revealed by sea-level observations. *Nature*, *521*(7553), 508–510. https://doi.org/10.1038/nature14491

Nnamchi, H. C., Li, J., Kucharski, F., Kang, I., Keenlyside, N. S., Chang, P., & Farneti, R. (2016). An equatorial–extratropical dipole structure of the Atlantic Niño. *Journal of Climate*, *29*, 7295–7311. https://doi.org/10.1175/JCLI-D-15-0894.1

Nnamchi, H. C., Li, J., Kucharski, F., Kang, I.-S., Keenlyside, N. S., Chang, P., & Farneti, R. (2015). Thermodynamic controls of the Atlantic Niño. *Nature Communications*, *6*, 8895. https://doi.org/10.1038/ncomms9895

Okumura, Y., & Xie, S.-P. (2004). Interaction of the Atlantic equatorial cold tongue and the African monsoon. *Journal of Climate*, *17*, 3589–3602. https://doi.org/10.1175/1520-0442(2004)017<3589:IOTAEC>2.0.CO;2

Polo, I., Dong, B. W., & Sutton, R. T. (2013). Changes in tropical Atlantic interannual variability from a substantial weakening of the meridional overturning circulation. *Climate Dynamics*, *41*(9-10), 2765–2784. https://doi.org/10.1007/s00382-013-1716-x

Pottapinjara, V., Girishkumar, M. S., Murtugudde, R., Ashok, K., & Ravichandran, M. (2019). On the relation between the boreal spring position of the Atlantic Intertropical Convergence Zone and Atlantic Zonal Mode. *Journal of Climate*, *32*, 4767–4781. https://doi.org/10.1175/JCLI-D-18-0614.1

Prodhomme, C., Voldoire, A., Exarchou, E., Deppenmeier, A.-L., García-Serrano, J., & Guemas, V. (2019). How does the seasonal cycle control equatorial Atlantic interannual variability? *Geophysical Research Letters*, *46*, 916–922. https://doi.org/10.1029/2018GL080837

Prigent, A., Lübbecke, J., Bayr, T., Latif, M., & Wengel, C. (2020). Weakened SST variability in the tropical Atlantic Ocean since 2000. *Climate Dynamics*, *54*(5–6), 2731–2744. https://doi.org/10.1007/s00382-020-05138-0

Rahmstorf, S., Box, J. E., Feulner, G., Mann, M. E., Robinson, A., Rutherford, S., & Schaffernicht, E. J. (2015). Exceptional twentieth-century slowdown in Atlantic Ocean overturning circulation. *Nature Climate Change*, *5*, 475–480. https://doi.org/10.1038/nclimate2554

Rayner, N. A., Parker, D. E., Horton, E. B., Folland, C. K., Alexander, L. V., Rowell, D. P., et al. (2003). Global analyses of sea surface temperature, sea ice, and night marine air temperature since the late nineteenth century. *Journal of Geophysical Research*, *108*(D14), 4407. https://doi.org/10.1029/2002JD002670

Reynolds, R. W., Rayner, N. A., Smith, T. M., Stokes, D. C., & Wang, W. (2002). An improved in situ and satellite SST analysis for climate. *Journal of Climate*, *15*, 1609–1625. https://doi.org/10.1175/1520-0442(2002)015<1609:AIISAS>2.0.CO;2

Richter, I., Behera, S. K., Masumoto, Y., Taguchi, B., Sasaki, H., & Yamagata, T. (2013). Multiple causes of interannual sea surface temperature variability in the equatorial Atlantic Ocean. *Nature Geoscience*, *6*, 43–47. https://doi.org/10.1038/ngeo1660

Richter, I., & Xie, S.-P. (2008). On the origin of equatorial Atlantic biases in coupled general circulation models. *Climate Dynamics*, *31*, 587–598. https://doi.org/10.1007/s00382-008-0364-z

Richter, I., Xie, S.-P., Behera, S. K., Doi, T. & Masumoto, Y. (2014). Equatorial Atlantic variability and its relation to mean state biases in CMIP5. *Climate Dynamics*, *42*, 171–188. https://doi.org/10.1007/s00382-012-1624-5

Robson, J., Ortega, P., & Sutton, R. (2016). A reversal of climatic trends in the North Atlantic since 2005. *Nature Geoscience*, *9*, 513–517. https://doi.org/10.1038/ngeo2727

Rossow, W. B., & Schiffer, R. A. (1999). Advances in understanding clouds from ISCCP. *Bulletin of the American Meteorological Society*, *80*, 2261–2288. https://doi.org/10.1175/1520-0477(1999)080<2261:AIUCFI>2.0.CO;2

Rotstayn, L. D., Jeffrey, S. J., Collier, M. A., Dravitzki, S. M., Hirst, A. C., Syktus, J. I., & Wong, K. K. (2012). Aerosol- and greenhouse gas-induced changes in summer rainfall and circulation in the Australasian region: A study using single-forcing climate simulations. *Atmospheric Chemistry and Physics*, *12*(14), 6377–6404. https://doi.org/10.5194/acp-12-6377-2012

Ruprich-Robert, Y., Msadek, R., Castruccio, F., Yeager, S., Delworth, T., & Danabasoglu, G. (2017). Assessing the climate impacts of the observed Atlantic multidecadal variability using the GFDL CM2. 1 and NCAR CESM1 global coupled models. *Journal of Climate*, *30*, 2785–2810. https://doi.org/10.1175/JCLI-D-16-0127.1

Schmidt, G. A., Ruedy, R., Hansen, J. E., Aleinov, I., Bell, N., Bauer, M., et al. (2006). Present day atmospheric simulations using GISS ModelE: Comparison to in-situ, satellite and reanalysis data. *Journal of Climate*, *19*(2), 153–192. https://doi.org/10.1175/JCLI3612.1

Sen, P. K. (1968). Estimates of the regression coefficient based on Kendall's tau. *Journal of the American Statistical Association*, *63*, 1379–1389. https://doi.org/10.2307/2285891

Servain, J., Caniaux, G., Kouadio, Y. K., McPhaden, M. J., & Aroujo, M. (2014). Recent climatic trends in the tropical Atlantic. *Climate Dynamics*, *43*(11), 3071–3089. https://doi.org/10.1007/s00382-014-2168-7

Stocker, T. F., Qin, D., Plattner, G.-K., Tignor, M., Allen, S. K., Boschung, J., Nauels, A., Xia, Y., Bex, V., & Midgley, P. M. (Eds) (2013). *IPCC, 2013: Climate Change 2013: The Physical Science Basis. Contribution of Working Group I to the Fifth Assessment Report of the Intergovernmental Panel on Climate Change* (p. 1535). Cambridge, United Kingdom and New York, NY, USA: Cambridge University Press.

Sun, C., Kucharski, F., Li, J., Jin, F.-F., Kang, I.-S., & Ding, R. (2017). Western tropical pacific multidecadal variability forced by the Atlantic Multidecadal Oscillation. *Nature Communications*, *8*, 15,998. https://doi.org/10.1038/ncomms15998

Svendsen, L., Kvamstø, N. G., & Keenlyside, N. (2014). Weakening AMOC connects equatorial Atlantic and Pacific interannual variability. *Climate Dynamics*, *43*(11), 2931–2941. https://doi.org/10.1007/s00382-013-1904-8

Taylor, K., Stouffer, R., & Meehl, G. (2012). An overview of CMIP5 and the experiment design. *Bulletin of the American Meteorological Society*, *93*, 485–498. https://doi.org/10.1175/BAMS-D-11-00094.1

Theil, H. (1950). A rank-invariant method of linear and polynomial regression analysis. *Proceedings of the Royal Netherlands Academy of Sciences*, *53*, 386–392.

Tokinaga, H., & Xie, S.-P. (2011). Weakening of the equatorial Atlantic cold tongue over the past six decades. *Nature Geoscience*, *4*, 222–226. https://doi.org/10.1038/ngeo1078

Voldoire, A., Sanchez-Gomez, E., Salas y Mélia, D., Decharme, B., Cassou, C., Sénési, S., et al. (2013). The CNRM-CM5.1 global climate model: Description and basic evaluation. *Climate Dynamics*, *40*(9-10), 2091–2121. https://doi.org/10.1007/s00382-011-1259-y

Wang, C., Zhang, L., Lee, S.-K., Wu, L., & Mechoso, C. R. (2014). A global perspective on CMIP5 climate model biases. *Nature Climate Change*, *4*, 201–205. https://doi.org/10.1038/nclimate2118

Watanabe, M., Chikira, M., Imada, Y., & Kimoto, M. (2011). Convective control of ENSO simulated in MIROC. *Journal of Climate*, *24*, 543–562. https://doi.org/10.1175/2010JCLI3878.1

Xie, S. P., & Carton, J. A. (2004). Tropical Atlantic variability: Patterns, mechanisms, and impacts. In *Earth's Climate: The ocean-atmosphere interaction* (pp. 121–142). Washington, DC: American Geophysical Union. https://doi.org/10.1029/147GM07

Xin, X., Tong-Wen, W., Jiang-Long, L., Zai-Zhi, W., Wei-Ping, L., & Fang-Hua, W. (2013). How well does BCC_CSM1.1 reproduce the 20th century climate change over China? *Atmospheric and Oceanic Science Letters*, *6*(1), 21–26. https://doi.org/10.1080/16742834.2013.11447053

Yan, X., Zhang, R., & Knutson, T. R. (2018). Underestimated AMOC variability and implications for AMV and predictability in CMIP models. *Geophysical Research Letters*, *45*, 4319–4328. https://doi.org/10.1029/2018GL077378

Yan, X., Zhang, R., & Knutson, T. R. (2019). A multivariate AMV index and associated discrepancies between observed and CMIP5 externally forced AMV. *Geophysical Research Letters*, *46*, 4421–4431. https://doi.org/10.1029/2019GL082787

Yu, L., & Weller, R. A. (2007). Objectively analyzed air-sea heat fluxes for the global ice-free oceans (1981–2005). *Bulletin of the American Meteorological Society*, *88*, 527–539. https://doi.org/10.1175/BAMS-88-4-527

Yukimoto, S., Hosaka, M., Sakami, T., Yoshimura, H., Hirabara, M., Tanaka, T. Y., et al. (2012). A new global climate model of the meteorological research institute: MRI-CGCM3—Model description and basic performance. *Journal of the Meteorological Society of Japan*, *90A*, 23–64. https://doi.org/10.2151/jmsj.2012-A02

Zebiak, S. (1993). Air–Sea Interaction in the Equatorial Atlantic Region. *Journal of Climate*, *6*(8), 1567–1586. https://doi.org/10.1175/1520-0442(1993)006<1567:aiitea>2.0.co;2

Zhang, R., & Delworth, T. (2007). Impact of the Atlantic Multidecadal Oscillation on North Pacific climate variability. *Geophysical Research Letters*, *34*, L23708. https://doi.org/10.1029/2007GL031601

Zhang, R., Delworth, T., Sutton, R., Hodson, D., Dixon, K., Held, I., et al. (2013). Have aerosols caused the observed Atlantic multidecadal variability? *Journal of the Atmospheric Sciences*, *70*(4), 1135–1144. https://doi.org/10.1175/jas-d-12-0331.1

Zuo, H., Balmaseda, M., Tietsche, S., Mogensen, K., & Mayer, M. (2019). The ECMWF operational ensemble reanalysis–analysis system for ocean and sea ice: A description of the system and assessment. *Ocean Science*, *15*(3), 779–808. https://doi.org/10.5194/os-15-779-2019